Molecular Counting & Single Molecule Localization Microscopy in Living Cells Using Deep-Learning

Mahzad Khoshlessan

Abstract

Single molecule localization microscopy (SMLM) is widely used to determine the organization and stoichiometry of protein complexes. The information obtained by counting methods is especially relevant in unraveling complex multi-protein processes. An important theoretical challenge arises from the fact that single molecules are only indirectly monitored through photons emitted from their fluorescent labels that, themselves, can exhibit complex photo-physics. Here, we introduce a specialized software for localization and molecular counting of SMLM data for biological interpretations. In this project it is tried to study, understand and produce the results presented in [1]. A deep convolutional neural network is used to quantify the number of particles in a region of interest (ROI). This method is parameter free and is able to overcome important theoretical challenge arises from the complex photo-physics of single molecules. We validate the code by super-resolution image reconstruction of simulated data from [1].

1. Introduction

1.1. Why Counting matters?

Super-resolution (SR) optical imaging is an important tool in biological discovery. Single molecule localization microscopy (SMLM) has evolved remarkably over the last decade and provides insight into cells at the level of its principle actors, i.e. single molecules. Counting problem has several advantages among which are: counting the number of protein complexes involved in cellular tasks

Email address: mkhoshle@asu.edu (Mahzad Khoshlessan)

[2], inferring protein complex stoichiometry in vivo [3, 4], determining complex's stoichiometry to understand its operation [5, 6], gaining insight into the biological effects of protein structures from their spatiotemporal ordering of its constituent proteins [7]. A reliable tool for quantitative analysis of SMLM data, is of great importance in supporting biological hypotheses tied to protein complex assemblies and ultimately unraveling complex multi-protein processes.

1.2. Counting Limitation

The quantitative analysis task can be very challenging due to different artifacts and is faced with different limitations. Biological constraints are one reason that complicates the counting problem. For instance, even if all proteins are labeled and are expressed in their native amount, not all PA-FPs mature [8, 9], nor will all PA-FPs successfully photoconvert [10]. Additionally, uncertainty in the localization of single molecules, sample drift during the long imaging time, and inaccurate image registration in the case of dual-color imaging are inherent sources of error in SMLM techniques [11].

Besides biological constraints, photo-activatable fluorescent proteins (PA-FPs) exhibit complex photo-physics. First of all their photo-physics and kinetic are not always known, second, reversible switches between active and dark states, also called photo-blinking, can lead to over-counting [12–14].

In addition, when multiple PA-FP spikes occur, overlapping and superposing signals arise over a short period which makes the counting problem complicated. This can happen due to multiple situations, e.g. when: (i) there are a large number of PA-FPs; (ii) the PA-FP blinking rate is fast and the PA-FP photobleaching rate is slow; and (iii) the PA-FP photo-activation rate is fast and the PA-FP photobleaching rate is slow [13].

Over-counting can also occur when target proteins are labeled with primary and secondary antibodies or when antibodies are conjugated to multiple fluorophores [12]. In addition, neighboring fluorescent probes can influence each other's photo-kinetics, resulting in different blinking behavior [15].

1.3. Previous approaches on counting

Thus far, there have been different attempts to deal with counting problem. However, each of these approaches come with their own limitations and constraints and does not appropriately address all of these limitations.

Counting from fluorescence intensity includes methods which rely on total observed intensity or a standard mean PA-FPs brightness. However, these methods have a low precision [16].

Counting by photobleaching using diffraction limited data is an alternative approach that rely on the stochastic photobleaching of single fluorophores. This approach assumes that the times at which multiple active fluorescent proteins appearing within the same diffraction spot eventually photo-bleach are stochastic and thus likely different from one another. Thus, a time series of the total fluorescence signal will exhibit a stepwise decrease [3]. However, the precisions of these models is dependent on the noise level in the data.

Step-finding algorithms to count the number of photobleaching steps is another method for counting the number of particles [17–19]. However the downside with these approaches is that a precise understanding of the noise characteristics in the data generating process is required to accurately locate steps.

Other approaches count molecules by means of photon arrival statistics [20, 21]. These techniques exploits the photon anti-bunching effect, which essentially states that a single emitting quantum system emits photons one at a time. However, this method is limited to counting up to 20 or so molecules, largely because of error introduced by blinking and photobleaching effects.

Other methods for counting by blinking correction use thresholding methods for counting from Photo-activated Localization Microscopy (PALM) data [13]. However, in the presence of blinking, counting remains possible so long as consecutive bursts originating from the blinking of a single fluorophore can be grouped together. Coltharp et al. [22] used a clustering algorithm to group localizations that originate from the same molecule using clustering thresholds (t_{Thresh} and d_{Thresh}) to account for photoblinking. Rollins et al. [13] introduce a stochastic approach based on aggregated hidden Markov model. This

approach takes blinking statistics into account and provides estimates of kinetic rates and number of particles for any number of particles and regardless of its photo-physical properties. However, this approach does not work very well for noisy data as it relies on thresholding for separation between different states. Other methods used in [14, 23, 24] used temporal thresholding to separate PA-FPs. However, these methods do not treat PA-FPs stochastically.

SR-Tesseler [25] uses Voronoi tessellation to automatically segment SMLM data and uses the coordinates of localized molecules for the analysis. SR-Tesseler allows quantification of molecular organization at various cellular levels and stoichiometry determination of both genetically and immuno-labeled proteins and is insensitive to cell shape, molecular organization, background and noise. However, the interpretation of the stoichiometry and counting from the number of localizations requires careful controls and calibration on well-characterized reference biological samples to avoid misinterpretations arising from varying labeling or photo-conversion efficiency or from incomplete protein folding. In addition, SR-Tesseler does not provide any information regarding the kinetic rates and dynamics of the fluorephores.

A number of post-processing software tools covering the various aspects of quantitative analysis of SMLM data have been recently developed [26–28]. These software packages provide powerful tools for quantitative analysis of SMLM data [11, 29]. However, many of these tools are known to be difficult to parametrize experimentally, and also difficult to generalize [25]. For example, *DBSCAN* allows the classification of particles in an image into clusters; however, it is sensitive to background noise.

In the present study, we use a super-resolution image reconstruction model using Deep Learning. This method is capable of creating a super-resolved image from the raw data directly which can further be used for counting and clustering purposes.

2. Materials & Methods

The kinetic model considered in most super-resolution studies has four states including photo-activated (I), active (A), dark (D), and photo-bleached (B). Once active, the PA-FP has two options: (i) it can blink possibly transitioning multiple times between the active and the dark state or (ii) it can irreversibly photo-bleach. Fluorescence is only detected from the active state, not in the other three states. The kinetic model for these transitions is shown in Figure 1.

To test the method for finding the super-resoved image which will contain information about the number of particles, number of clusters, number of particles per cluster we analyzed sample simulated data, representing kinetic model of PA-FPs shown in Figure 1. These simulated trajectories (a sample of which is shown in Fig. fig:output (left)) were generated using the HMM stochastic simulation algorithm using the code given in [1].

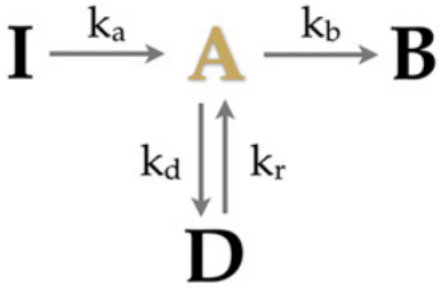

Figure 1: Kinetic model for PA-FP blinking. This kinetic model has four states inactive (I), active (A), dark (D), and photo-bleached (B). The only fluorescent state is A. We name the transitions between states this way: activation I $\rightarrow$ A, blinking A$\rightarrow$ D, recovery D$\rightarrow$ A, and photo-bleaching A$\rightarrow$ B [13].

2.1. NEURAL NETWORK ARCHITECTURE

The net architecture is based on a fully convolutional auto-encoder network. The network (Fig. 2) first encodes the input intensity image into a dense, aggregated feature representation. Afterwards, in the decoding stage, the spatial

dimensions are restored to the size of the input image through successive deconvolution layers.

In this study, a set of low-resolution diffraction limited images of stochastically blinking emitters (single molecule) is fed into the network to produce reconstructed high-resolution images. The resulting outputs are then summed to generate the final super-resolved image.

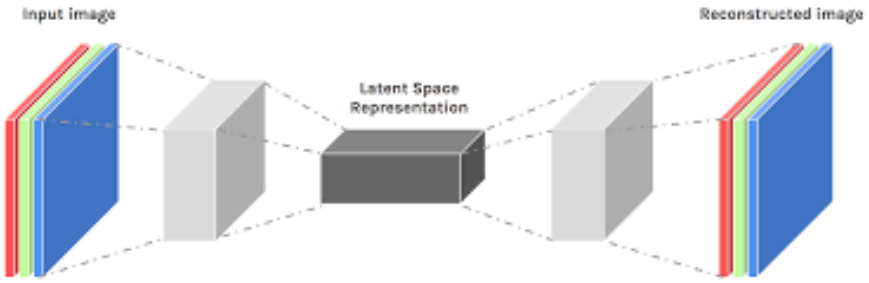

Figure 2: Network architecture.

The network architecture used in the [1] for the reconstruction of high-resolution super-resolved images is shown in Figure 3. Convolutional layers, for both encoding and decoding, are followed by batch normalization, and then a ReLU nonlinearity.

2.1.1. Training

Training and evaluation were run on ASU Supercomputing Cluster, Agave. The jobs were run on x86 compute nodes which contain two Intel Xeon E5-2680 v4 CPUs running at 2.40GHz and 4 TB of RAM. The dataset used in this project is chosen from the available datasets provided in [1]. Then the simulated images are created using the codes provided in the study by NEHME et al [1]. The dataset is a set of 10,000 low-resolution regions (208×208 pixels), with spikes at the ground truth positions used as training examples. The 10K regions were split into a 7000 training set, and 3000 validation set to prevent over-fitting. Details of the hyper-parameters used in the convolutional network and the loss function is given in Table 1.

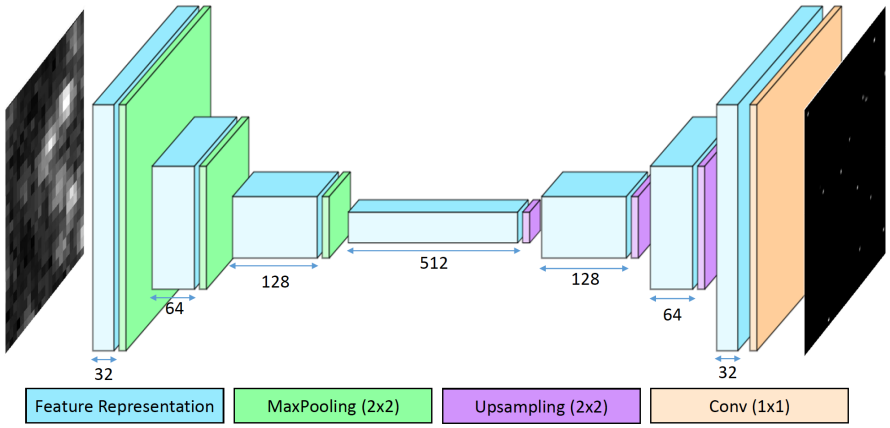

Figure 3: Fully convolutional architecture details. The number below each Feature Representation block refers to the number of convolutional filters in the respective convolutional layer. Size of the convolutional filters is 3×3. Therefore, the network has only about 1.3M trainable parameters [1].

Parameters	**Value**
Learning rate	0.001
Batch size	16
Number of epochs	100
Train Size	7000
Test Size	3000
Initialization	Orthogonal weight matrices
Optimizer	Adam
Loss function	$l(x,\hat{x}) = \frac{1}{N}\sum_{i=1}^{N} \|\hat{x}_i \circledast g - x_i \circledast g\|_2^2 + \|\hat{x}_i\|_1$

Table 1: Summary of the hyper-parameters used in convolutional network

All codes for Keras and PyTorch implementations along with the codes to create the input datasets and all the outputs from the present study are available in the repository of the report.

3. Comparison of Loss Values Between Keras and Pytorch Implementations

The comparison between the calculated loss values are shown in Figure 4. The Keras implementation is the original implementation used in the [1]. As can be seen the Training and Test loss decrease with the number of epochs and

there is a small difference between the two losses which suggest that we have a good fit. PyTorch implementation is the present project's attempt to understand the code and reproduce the original results in [1]. It seems that the PyTorch implementation is doing a good job at training time, but the test loss does not decrease much and suggest some overfitting or bug in the PyTorch implementations. All the weight vectors from both models are double checked and everything looks fine, which suggests that there is not any error in the architecture of the neural network for the PyTorch implementation. The effect of removing the scheduler and orthogonal weight initialization on PyTorch implementation performance is also studied. As can be seen in Figure 4 removing the scheduler and orthogonal weight initialization does not improve the behavior of the PyTorch implementation. This also suggests that there might be differences in the implementations of the two packages or a small bug in the PyTorch implementation. However, at this point it is not very well clear to me what might cause the overfitting in the PyTorch implementation.

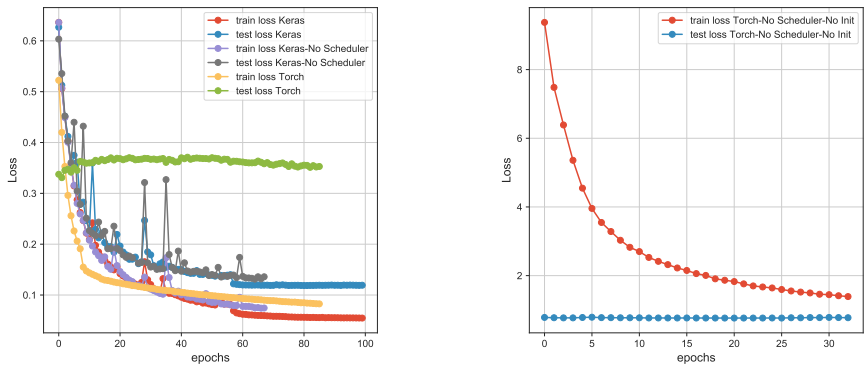

(a) Loss Comparison 1

(b) Loss Comparison 2

Figure 4: Performance comparison between Keras and PyTorch implementations. All the hyper parameters for these calculations are given in Table 1

3.1. Sample Output for the Synthetic Data Used as Dataset in the Present Study

It should be noted that the dataset is trained without any additional data augmentation. An example training input image and the corresponding output (after training) are shown in Figure 5. The figure on the left is the simulated low-resolution image and the one on the right hand side is the convolutional network prediction.

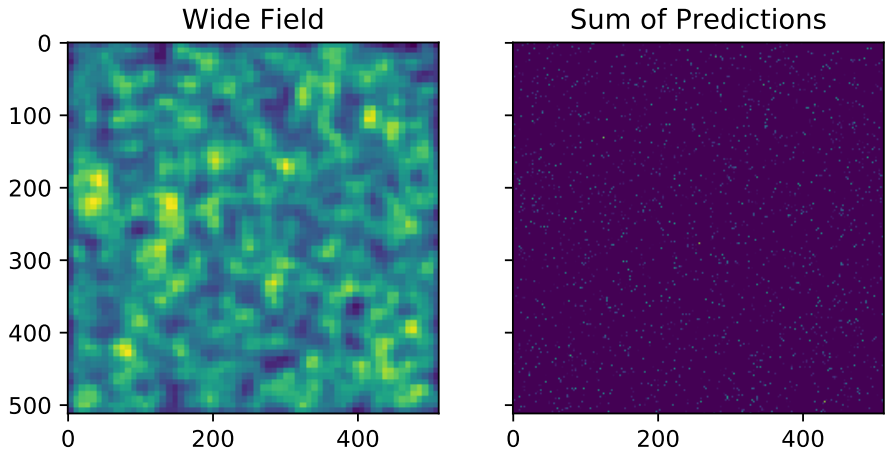

Figure 5: Simulated dense emitters. (a) Low-resolution image obtained from simulated data. (b) Deep-STORM prediction with ground truth emitter locations overlaid as cross marks on top. The outputs are obtained using Keras implementation.

4. Conclusion

Deep-STORM implicitly uses the low resolution image content to directly reconstruct a super resolved image. The technique combines state-of-the-art resolution enhancement, unprecedented speed, and high flexibility (parameter-free operation). Both Keras and PyToch implementations are used for training. Keras implementation provides a very good fit. The PyTorch results suggest overfitting or a bug in the PyTorch implementation which requires further debugging. The expected outcome is that both implementation will have comparable results which is not the case with the current version.

References

1. NEHME, E., WEISS, L.E., MICHAELI, T., SHECHTMAN, Y.. Deep-storm: super-resolution single-molecule microscopy by deep learning. Optica 2018;5(4).
2. Berg, H.. The rotary motor of bacterial flagella. Annual Review of Biochemistry 2003;72:19–54.
3. Leake, M., Chandler, J., Wadhams, G., Bai, F., Berry, R., Armitage, J.. Stoichiometry and turnover in single, functioning membrane protein complexes. Nature 2006;443:355–358.
4. Delalez, N.J., Wadhams, G.H., Rosser, G., Xue, Q., Brown, M.T., Dobbie, I.M., et al. Signal-dependent turnover of the bacterial flagellar switch protein flim. Proceedings of the National Academy of Sciences of the United States of America 2010;107:11347–11351.
5. Wu, L., Lewis, P., Allmansberger, R., Hauser, P., Errington, J.. A conjugation-like mechanism for prespore chromosome partition- ing during sporulation in bacillus subtilis. Genes Dev 1995;9:1316–1326.
6. Liu, N., Dutton, R., Pogliano, , Evidence, K.. That the spoiiie dna translocase participates in membrane fusion during cytokinesis and engulfment. Molecular Microbiology 2006;28:9–22.
7. Baker, M., Wolanin, P., Stock, J.. Signal transduction in bacterial chemotaxis. BioEssays 2006;28:9–22.
8. M., U., E., I.. Subunit counting in membrane-bound proteins. Nature Methods 2007;4:319–321.
9. C., S.N., A., S.P., A, T.R.Y.. Guide to choosing fluorescent proteins. Nature Methods 2005;2:905–909.
10. N., D., L., L.C., A., S.A., J., B., M., L.. Single-molecule evaluation of fluorescent protein photoactivation efficiency using an in vivo nanotemplate. Nature Methods 2014;11:156–62.
11. Deschout, H., Shivanandan, A., Annibale, P., Scarselli, M., Radenovic, A.. Progress in quantitative single-molecule localiza-

tion microscopy. Histochemistry and Cell Biology 2014;142(1):5–17. URL: http://dx.doi.org/10.1007/s00418-014-1217-y. doi:10.1007/s00418-014-1217-y.

12. Veatch, S.L., Machta, B.B., Shelby, S.A., Chiang, E.N., Holowka, D.A., Baird, B.A.. Correlation functions quantify super-resolution images and estimate apparent clustering due to over-counting. PLoS ONE 2012;7(2):e31457. URL: http://dx.doi.org/10.1371/journal.pone.0031457. doi:10.1371/journal.pone.0031457.

13. Rollins, G.C., Shin, J.Y., Bustamante, C., Pressé, S.. Stochastic approach to the molecular counting problem in superresolution microscopy. Proceedings of the National Academy of Sciences 2014;112(2):E110–E118. URL: http://dx.doi.org/10.1073/pnas.1408071112. doi:10.1073/pnas.1408071112.

14. Lee, S.H., Shin, J.Y., Lee, A., Bustamante, C.. Counting single photoactivatable fluorescent molecules by photoactivated localization microscopy (palm). Proceedings of the National Academy of Sciences 2012;109(43):17436–17441. URL: http://dx.doi.org/10.1073/pnas.1215175109. doi:10.1073/pnas.1215175109.

15. Baddeley, D., Bewersdorf, J.. Biological insight from super-resolution microscopy: What we can learn from localization-based images. Annual Review of Biochemistry 2018;87:965–989.

16. Lee, A., Tsekouras, K., Calderon, C., Bustamante, C., Pressé, S.. Unraveling the thousand word picture: An introduction to super-resolution data analysis. Chemical Review 2017;117(11):pp 7276–7330.

17. K., T., C., C.T., H., J., G., W.N., S, P.. A novel method to accurately locate and count large numbers of steps by photobleaching. Mol Biol Cell 2016;27:3601–3615.

18. Y., C., N., D., C., A., W., H.. Molecular counting by photobleaching in protein complexes with many subunits: Best practices and application to the cellulose synthesis complex. Mol Biol Cell 2014;25:3630–3642.

19. H.b, M., M., A., Bowie, D., R., B.. Automating single subunit

counting of membrane proteins in mammalian cells. Journal of Biological Chemistry 2012;287:35912–35921.

20. W., A., P., G., J., E., D., S., J., M., R., K.. Fluorescence photon antibunching from single molecules on a surface. Chemical Physics Letters 1997;269:365–370.

21. A., K., J., S., K., G., P., H., P., T., D.P., H.. Counting fluorescent dye molecules on dna origami by means of photon statistics. Small 2013;9:4061–4068.

22. Coltharp, C., Kessler, R.P., Xiao, J.. Accurate construction of photoactivated localization microscopy (palm) images for quantitative measurements. PLoS ONE 2012;7(12):e51725. URL: http://dx.doi.org/10.1371/journal.pone.0051725. doi:10.1371/journal.pone.0051725.

23. Annibale, P., Vanni, S., Scarselli, M., Rothlisberger, U., Radenovic, A.. Identification of clustering artifacts in photoactivated localization microscopy. Nature Methods 2011;8(7):527–528. URL: http://dx.doi.org/10.1038/nmEth.1627. doi:10.1038/nmeth.1627.

24. Annibale, P., Vanni, S., Scarselli, M., Rothlisberger, U., Radenovic, A.. Quantitative photo activated localization microscopy: Unraveling the effects of photoblinking. PLoS ONE 2011;6(7):e22678. URL: http://dx.doi.org/10.1371/journal.pone.0022678. doi:10.1371/journal.pone.0022678.

25. Levet, F., Hosy, E., Kechkar, A., Butler, C., Beghin, A., Choquet, D., et al. Sr-tesseler: a method to segment and quantify localization-based super-resolution microscopy data. Nature Methods 2015;12(11):1065–1071. URL: http://dx.doi.org/10.1038/nmeth.3579. doi:10.1038/nmeth.3579.

26. Malkusch, S., Heilemann, M.. Extracting quantitative information from single-molecule super-resolution imaging data with lama – localization microscopy analyzer. Scientific Reports 2016;6(1). URL: http://dx.doi.org/10.1038/srep34486. doi:10.1038/srep34486.

27. Pengo, T., Holden, S.J., Manley, S.. Palmsiever: a tool to turn raw data into results for single-molecule localization microscopy. Bioinformatics 2014;31(5):797–798. URL: http://dx.doi.org/10.1093/bioinformatics/btu720. doi:10.1093/bioinformatics/btu720.

28. Andronov, L., Lutz, Y., Vonesch, J.L., Klaholz, B.P.. Sharpvisu: integrated analysis and segmentation of super-resolution microscopy data. Bioinformatics 2016;32(14):2239–2241. URL: http://dx.doi.org/10.1093/bioinformatics/btw123. doi:10.1093/bioinformatics/btw123.

29. Nan, X., Collisson, E.A., Lewis, S., Huang, J., Tamguney, T.M., Liphardt, J.T., et al. Single-molecule superresolution imaging allows quantitative analysis of raf multimer formation and signaling. Proceedings of the National Academy of Sciences 2013;110(46):18519–18524. URL: http://dx.doi.org/10.1073/pnas.1318188110. doi:10.1073/pnas.1318188110.